Supporting Information:

Toward an Internally Consistent Model for Hg(II) Chemical Speciation Calculations in Bacterium–Natural Organic Matter–Low Molecular Mass Thiol Systems

Yu Song,[*,†] Gbotemi A. Adediran,[‡,§] Tao Jiang,[†] Shusaku Hayama,[¶] Erik Björn,[‡] and Ulf Skyllberg[*,†]

†*Department of Forest Ecology and Management, Swedish University of Agricultural Science, SE-901 83 Umeå, Sweden*

‡*Department of Chemistry, Umeå University, SE-901 87 Umeå, Sweden*

¶*Diamond Light Source, Didcot, Oxfordshire OX11 0DE, United Kingdom*

§*Current address: Department of Soil and Environment, Swedish University of Agricultural Science, SE-750 07 Uppsala, Sweden*

E-mail: yu.song@slu.se; ulf.skyllberg@slu.se

Phone: +46 (0)90-786 84 60

This supporting information contains text, three tables and seven figures.

Bacterial Cultures and Membranes Isolation

Geobacter sulfurreducens PCA[S1] (purchased from DSMZ, Braunschweig, Germany) was cultured in a MOPS buffered medium under fumarate reducing condition at 28 °C, pH 6.8 as described in previous studies.[S2] The medium contained 1 g L^{-1} yeast extract, 40 mM sodium fumarate, 10 mM MOPS, 10 mM sodium acetate, 5 mM NH_4Cl, 1.3 mM KCl, 0.25 mM $MgSO_4$, 0.17 mM NaCl, 80 µM nitrilotriacetic acid, 50 µM NaH_2PO_4, 8.8 µM $CaCl_2$, 1 mg L^{-1} resazurin and trace metals which contained 30 µM $MnCl_2$, 4.2 µM $CoCl_2$, 3.6 µM $FeSO_4$, 3.5 µM $ZnSO_4$, 0.6 µM Na_2SeO_3, 0.4 µM $NiCl_2$, 0.4 µM Na_2MoO_4, 0.04 µM $CuSO_4$. *Desulfovibrio desulfuricans* ND132 (obtained from C. Gilmour, Smithsonian Environmental Research Center, U.S.) was anaerobically cultured at 30 °C, pH 7.2 in a low sulfate medium as described previously.[S3] The medium contained 2 g L^{-1} yeast extract, 60 mM DL-Lactic acid, 30 mM Tris buffer, 170 mM NaCl, 30 mM Na_2SO_4, 8 mM $MgCl_2$, 5 mM NH_4Cl, 2 mM KH_2PO_4, 0.6 mM $CaCl_2$, 0.12 mM EDTA, 1 mg L^{-1} resazurin and trace metals which contained 15 µM $MnCl_2$, 8.8 µM $ZnSO_4$, 7.6 µM $CoCl_2$, 6 µM $FeCl_2$, 2.3 µM $NiCl_2$, 1.9 µM HBO_3, 1.3 µM Na_2MoO_4, 0.07 µM $CuSO_4$, 0.036 µM Na_2SeO_3. Cells of *Geobacter* and ND132 were harvested at late exponential phase (OD_{660} ~0.5) by centrifugation at 4000 g for 30 min (Mega Star 1.6R, VWR®) and washed with carbon free assay buffer solution GsAB and DdAB, respectively for at least three times. The assay buffer, GsAB, for *Geobacter* was free of carbon source, modified from Schaefer and Morel containing 10 mM MOPS, 5 mM NaH_2PO_4, 1.3 mM KCl, 0.17 mM NaCl, 0.15 mM $MgSO_4$, 0.1 mM NH_4Cl and 1 mg/L resazurin; DdAB for ND132 was free of carbon source and sulfate, modified from Schaefer et al. containing 10 mM MOPS, 170 mM NaCl, 0.5 mM KCl, 0.4 mM $MgCl_2$, 0.2 mM KH_2PO_4, 0.1 mM NH_4Cl and 1 mg/L resazurin.

To expose all accessible thiol groups on both inner and outer cell membranes,[S4,S5] the membrane isolation procedure was modified from standard protocols for targeting and isolating specific Gram-negative membrane proteins.[S5] Briefly, cells were first subjected to physical lysing by freeze-thaw and ultrasonic treatment. The cellular debris was centrifuged at 4000 g for 30 min to remove unbroken cells before subjecting the supernatant fluid to ultracentrifugation at 160 000 g for 40 min

(Beckman, Ti70 rotor). The obtained pellet was vortexed after rinsed with deoxygenated Milli-Q water to wash away intracellular thiols not associated with membranes. We vortexed the membrane pellet instead of using Triton X-100 solution (which can permeabilize the membrane) of the standard protocol since we were not targeting the membranes proteins, moreover, we avoided to modify the membrane structure as much as possible. Extracellular metabolites were isolated from cells by filtering the culture media through 0.2-µm filters (Filtropur S, Sarstedt) in a N_2-filled glovebox after 6 h of cell incubation (3.8×10^8 cells mL^{-1}) in assay buffer solutions GsAB and DdAB.

X-ray Absorption Spectroscopy Analyses

Sulfur K-edge XANES spectra were collected at Beamline 4B7A in Beijing Synchrotron Radiation Facilities (BSRF), China. The experiment was conducted in fluorescence mode with a Si(111) double crystal monochromator at ambient temperature under high vacuum (10^{-8}–10^{-6} mbar). In order to protect the samples from oxidation, the culture media, buffer assays and any solution used were deoxygenated. The preparation processes (cells harvest, membranes extraction) were conducted in the glovebox, and the samples were protected from light by covering the vessels with aluminum foils. The freeze-dried samples were quickly put back into the glovebox for more than 2 h (with vessels lids opened) to build a N_2(g) atmosphere for the samples. The samples were then stored in a –20 °C freezer until analysis. Radiation damage was monitored by comparing successive scans. No radiation damage was observed. High self-absorption effects of several high sulfur concentration samples were observed and these samples were diluted in boron nitride (BN) and measured again. Scans were taken at the energy range of 2462–2500 eV with a step size of 0.2 eV. Data averaging, normalization, and Gaussian curve deconvolution were conducted using Athena, WinXAS and Microsoft Excel, respectively,[S6–S8] following the procedure in Song et al..

Mercury L_{III}-edge EXAFS spectra were collected in fluorescence mode using a four-bounce Si(111) monochromator equipping with a 64-element solid state Ge detector on Beamline I20-scanning at Diamond Light Source, U.K..[S10] The X-ray source is derived from a wiggler insertion

device giving a spot size of 400 × 300 µm ($h \times v$) at the sample position. The sample was mounted in a flat PEEK holder, sealed with two Kapton® foil windows and determined at 77 K in a liquid nitrogen (LN_2) cryostat (Optistat DN2, Oxford Instruments). The Hg L_{III}-edge of 12 284 eV was calibrated at the Au L_{III}-edge of 11 919 eV with a gold foil. EXAFS data were collected in steps of 0.3 eV from 12 245 to 12 340 eV. One to three scans were collected and averaged by software Athena.[S7] Data were normalized in the energy range 12 200–12 600 eV and background was removed with a 7- or 8-knot spline function over the k-range 2.7–13.5 Å^{-1} (see Table 1). Data were reduced and fitted in Fourier Transformed R-space by a first coordination shell model using WinXAS[S11] and FEFF-7.[S12,S13] Models included Hg−S and Hg−O/N single paths in the first coordination shell, and the multiple scattering (MS) of Hg−S path: four-legged Hg−S−Hg−S−Hg and three-legged Hg−S−S−Hg, in agreement with models used for Hg(II)–NOM complexation.[S14]

Hg L_{III}-Edge EXAFS Determination of Thiols in Bacteria Membranes

As shown in Table 1 and Figure S4, at sufficiently low Hg_{tot} concentration (4 µmol g^{-1} C) not to saturate Mem-R^{II}S functional groups, Hg(II) forms a two-coordinated, linear complex with Mem-R^{II}S, Hg(Mem-R^{II}S)$_2$. This structure require the Mem-R^{II}S functional groups to be close and flexible enough to form the Hg(Mem-R^{II}S)$_2$ structure. At the increased Hg(II) additions of 28 and 55 µmol g^{-1} C, Hg EXAFS results suggests a significant contribution form RO/N functionalities in the complexation of Hg(II). Because the log K of Hg(II) to RO/N functionalities is expected to be ~20 orders of magnitude smaller than the Hg(Mem-R^{II}S)$_2$ complex, this can only be explained by a saturation of the Mem-R^{II}S functional groups. Hg(II) is always at least coordinated by two atoms, this may further suggest a formation of a mixed complex involving Mem-RSH groups and neighboring RO/N functional groups. These Mem-RSH groups are designated Mem-R^{I}S and the mixed complex Hg(Mem-R^{I}SRO). Finally, when all Mem-R^{I}S functional groups are saturated, Hg(II) is forming the Hg(Mem-RO)$_2$ structure, composed of only RO/N functionalities. The saturated

concentration of Mem-$R^{II}S$ may be calculated using the Hg L_{III}-edge EXAFS results as follows:

$$x_0 + y = Hg_{tot} \tag{1}$$

$$\frac{2x_0 + y}{y} = \frac{CN_S}{CN_O} \tag{2}$$

In Equation 1, Hg_{tot} denotes the total Hg concentration, x_0 denotes the concentration of Hg(Mem-$R^{II}S)_2$ when Mem-$R^{II}S$ is fully saturated. The total concentration of Mem-$R^{II}S$ groups equals $2x_0$. Equations 1 and 2 can be used to calculate y, representing the concentration of the Hg(Mem-$R^{I}SRO$) complex when the Mem-RS^{I} groups are not fully saturated. At higher Hg_{tot} concentrations, when both Mem-$R^{II}S$ and Mem-RS^{I} get saturated, the concentration of Mem-RS^{I} can be calculated by Equations 3 and 4:

$$x_0 + y_0 + z = Hg_{tot} \tag{3}$$

$$\frac{2x_0 + y_0}{y_0 + 2z} = \frac{CN_S}{CN_O} \tag{4}$$

where y_0 denotes the concentration of Hg(Mem-$R^{I}SRO$) when Mem-RS^{I} is fully saturated by Hg(II). The Mem-RS^{I} concentration equals to y_0. z denotes the concentration of Hg(Mem-RO)$_2$ when Mem-RO is not fully saturated.

Experimental Losses of Hg(II)

We observed an average loss of ~20% Hg_{tot} in the CLE experiments (Figure S2) with *Geobacter* membrane concentrations of 4–19 mg C L^{-1} (corresponding to a Hg(II)/Mem-RS_{tot} molar ratios

of 0.07–0.3). Similar to the CLE experiments, we also encountered significant losses of Hg_{tot} (13–64%) in samples subjected to Hg EXAFS experiments (Table 1). Notably, Hg^0 was not detected by EXAFS in any sample. Thus, Hg^0 was likely formed prior to EXAFS measurements, similar to experiences from Hg–NOM studies.[S9] As shown in Figure S3, the loss of Hg(II) was positively related to the Hg(II)/Mem-RS_{tot} molar ratio (as exemplified by the simple, linear equation: $y = 0.13x + 0.2$, $R^2 = 0.72$), which is consistent with previous Hg–NOM studies of dark, abiotic Hg(II) reduction.[S9,S15–S17] In presence of NOM, the rate of reduction increases with decreasing bonding strength between Hg(II) and NOM functional groups, which in turn correlates positively with the Hg(II)/NOM molar ratio. Redox active groups of NOM (e.g., quinone, phenolic, carboxylic and amide moieties) quickly reduce Hg(II) under conditions when Hg(II) loading exceeds the concentration of NOM-RSH and some Hg(II) is complexed by O/N functionalities.[S18] At lower Hg(II)/NOM-RSH ratios, when the Hg(NOM-$RS)_2$ structure is in control of the chemical speciation, the reduction is inhibited.[S16–S18] Inhibition was also demonstrated in our CLE experiment after the addition of Cys, when no further reduction of Hg(II) was observed (data not shown), well in agreement with the high dominance of the Hg(II) reduction resisting $Hg(Cys)_2$ and Hg(Mem-$RS)_2$ species.

Even if the mechanism of dark, abiotic reduction of Hg(II) at bacterial membranes remains to be studied, we know that phenolic, carboxylic and amide moieties are main functional groups of membranes[S19–S21] and our observed increase in Hg(II) reduction with increasing Hg(II) loading likely have a similar explanation as in experiments of dark Hg(II) reduction by NOM. Consequently, in studies of Hg(II) biotic reduction by *Geobacter*, Hu et al. found the reduction of Hg(II) to be suppressed at high cell concentration (i.e. at low Hg(II)/Mem-RS_{tot} ratios). Lin et al. reported that *Geobacter* can both reduce and oxidize Hg (depending on Hg/cell ratios). The reaction shifted from oxidation to reduction with increasing of Hg/cell ratios. Notably, in both studies abiotic reduction of Hg(II) by heat killed cells was observed (10–20%, depending on the Hg/cell ratios), in agreement with the losses in our membrane experiments. Interestingly, we found the largest loss of Hg(II) (35–64%) when complexed to the membrane of ND132. This bacterium has been reported to

oxidize Hg(0) to Hg(II),[S24] but the oxidation mainly occurred in the spheroplast while the cell wall fragments barely oxidized Hg(0).[S24]

Comparison of Thermodynamic Stabilities of the Protonated Form of Thiols

To improve the comparison of thermodynamic stabilities of the various complexes, differences in the pK_a values of Cys, NOM-RSH and Mem-RSH should be taken into account. This can be achieved by writing the reaction of Hg(II) with thiols in their protonated form: $Hg^{2+} + 2\,RSH \rightleftharpoons Hg(RS)_2 + 2\,H^+$ or $Hg^{2+} + HCys + RSH \rightleftharpoons Hg(Cys)(RS) + 2\,H^+$, where RSH represents any form of protonated thiols (HCys, NOM-RSH or Mem-RSH) and Hg(Cys)(RS) represents any of the mixed complexes Hg(Cys)(NOM-RS) or Hg(Cys)(Mem-RS). The log K values for $Hg(RS)_2$: $Hg(Cys)_2$, $Hg(NOM\text{-}RS)_2$ and $Hg(Mem\text{-}R^{II}S)_2$ calculated in this way are 20.3, 20.0 and 20.1, respectively, and the log K values for mixed complexes Hg(Cys)(NOM-RS) and $Hg(Cys)(Mem\text{-}R^{I}S)$ are 19.9 and 20.5, respectively. The small differences among these constants suggests that all these complexes in essence have quite equal thermodynamic stabilities at pH values when the thiol groups are protonated.

Table S1: Selected Chemical Reactions and Thermodynamic Constants (log K ± SD) Used in the Chemical Speciation Modeling

Reaction		**log K**	**Reference**
$HCys^{\S} \rightleftharpoons H^+ + Cys^-$	(1)	−8.6	S25
$NOM\text{-}RSH \rightleftharpoons H^+ + NOM\text{-}RS^-$	(2)	−10	S26
$Mem\text{-}RSH \rightleftharpoons H^+ + Mem\text{-}RS^-$	(3)	−9.5 ± 0.2	S27
$Hg^{2+} + 2\,Cys^- \rightleftharpoons Hg(Cys)_2$	(4)	37.5 ± 0.2	S25
$Hg^{2+} + Cys^{2-} \rightleftharpoons HgCys^{\dagger}$	(5)	24	S9
$Hg^{2+} + 2\,NOM\text{-}RS^- \rightleftharpoons Hg(NOM\text{-}RS)_2$	(6)	40.0 ± 0.2	S9
$Hg^{2+} + NOM\text{-}RSRO^{2-} \rightleftharpoons Hg(NOM\text{-}RSRO)$	(7)	26	S9
$Hg^{2+} + Cys^- + NOM\text{-}RS^- \rightleftharpoons Hg(Cys)(NOM\text{-}RS)$	(8)	38.5 ± 0.2	S9
$Hg^{2+} + 2\,Mem\text{-}R^{II}S^- \rightleftharpoons Hg(Mem\text{-}R^{II}S)_2$	(9)	39.1 ± 0.2 ‡	This study
$Hg^{2+} + Cys^- + Mem\text{-}R^{I}S^- \rightleftharpoons Hg(Cys)(Mem\text{-}R^{I}S)$	(10)	38.1 ± 0.1 ‡	This study
$Hg^{2+} + Mem\text{-}R^{I}SRO^{2-} \rightleftharpoons Hg(Mem\text{-}R^{I}SRO)$	(11)	25.6 ± 0.1‡	This study

§ HCys denotes $HSCH_2CH(NH_3^+)COO^-$ with the carboxyl group deprotonated ($-COO^-$), and the thiol ($-SH$) and amino groups ($-NH_3^+$) protonated; Cys^- denotes $(S^-)CH_2CH(NH_3^+)COO^-$ with both the carboxyl ($-COO^-$) and thiol ($-S^-$) groups deprotonated.

† HgCys means the mix complex of Hg with one RS and one RO/N groups that are in the same Cys molecule.

‡ denotes the membranes samples of *Geobacter*. The log K values for ND132 are 39.2 ± 0.2, 38.2 ± 0.1 and 25.7 ± 0.1, respectively.

Table S2: Sulfur Chemical Species Percentage (%) in Samples of Whole Cells, Isolated Membranes and Extracellular Metabolites of *Geobacter* and ND132 Determined by S K-Edge XANES

	Geobacter			**ND132**		
	Cell	Membrane	Extracellular	Cell	Membrane	Extracellular
Sulfide	6	0	0	10	0	0
Zero-valent S	2	6	7	9	8	3
Disulfide	3	13	13	7	12	8
Monosulfide + Thiol	82	76	12	59	54	10
Sulfonate	3	3	47	10	16	58
Sulfate	2	2	21	6	10	20
Org-S_{RED}[†]	89	86	25	67	65	18

[†] denotes reduced organic sulfur, the sum of thiol (RSH), monosulfide (RSR) and disulfide (RSSR). The uncertainty for the reported data is ~5%.

Table S3: Data on cell membrane thiol concentrations of *Geobacter* and ND132

Bacterium	Wet μmol g^{-1} cell	Dry μmol g^{-1} C	Wet/Dry μmol $cell^{-1}$	Method	Reference
Geobacter	/	380[§]	3.8×10^{-11}[‡]	Hg L_{III}-edge EXAFS	This study
	240	2000*	/	Fluorescence (qBBr)	S27
	67.8	550*	/	Potentiometric titration	S27
	55.5	466*	3.3×10^{-10}[†]	Fluorescence (qBBr)	S28
	0.07	0.6*	3.4×10^{-14}[†]	Fluorescence (ThioGlo-1)	S29
ND132	/	350[§]	2.8×10^{-9} [‡]	Hg L_{III}-edge EXAFS	This study
	/	/	2.8×10^{-12} [‡]	Fluorescence (TFP-4)	S24

Wet denotes wet weight and Dry denotes dry weight.
[§] the average thiol concentration of inner and outer membranes.
* outer membrane thiol concentrations re-calculated from other studies (in the unit of μmol g^{-1} wet cells), assuming a TOC content of 50% and a wet/dry ratio of 4.2 reported by Mishra et al..[S27]
[†] data represent the outer cell membrane.
[‡] data represent the average of inner and outer membranes.

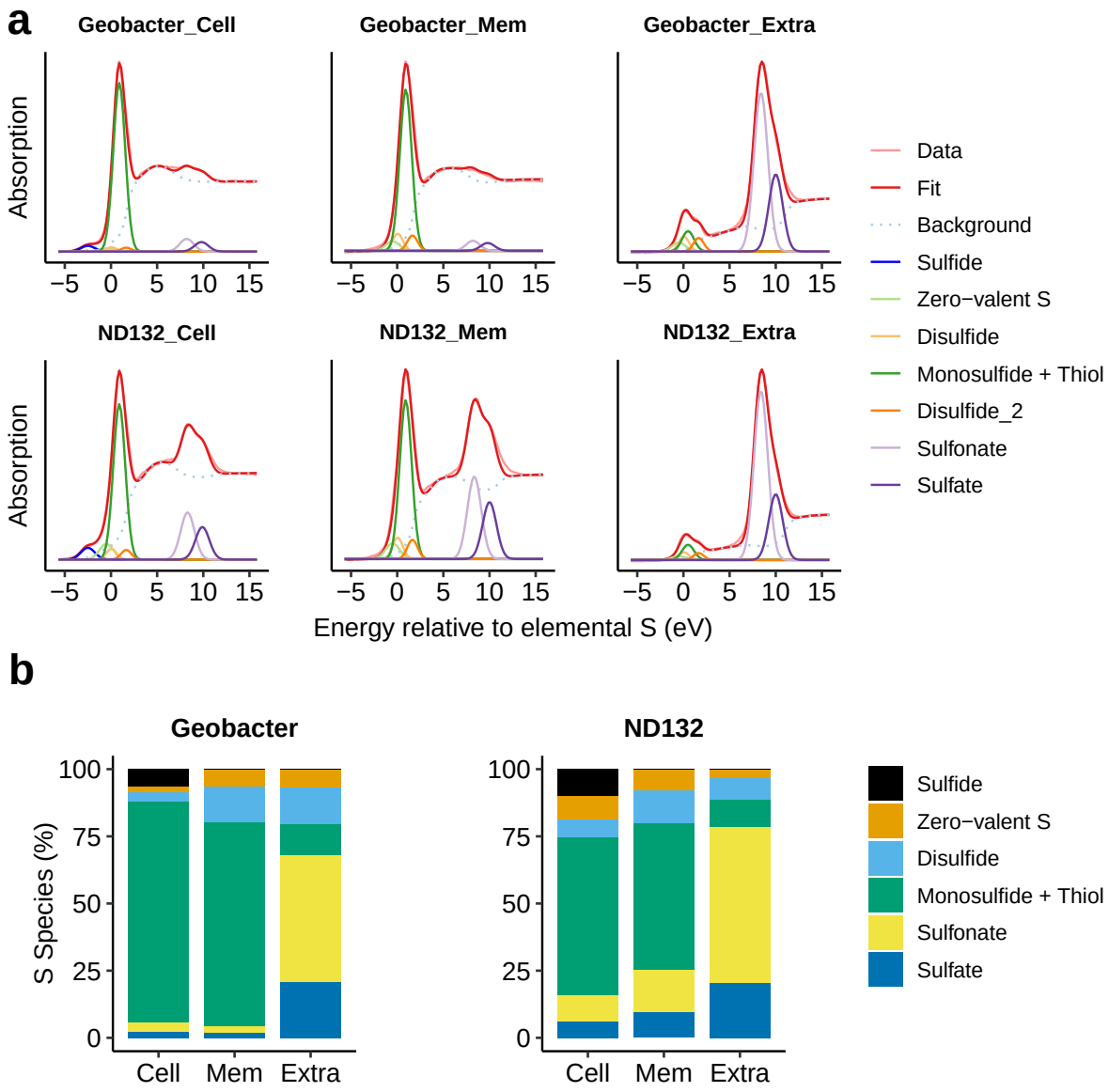

Figure S1: (a) Sulfur K-edge XANES spectra and Gaussian curve pseudo-component fits, and (b) sulfur speciation (percentage of total S, %) in samples of whole cells (Cell), isolated membranes (Mem), and extracellular metabolites (Extra) of bacteria *Geobacter* and ND132.

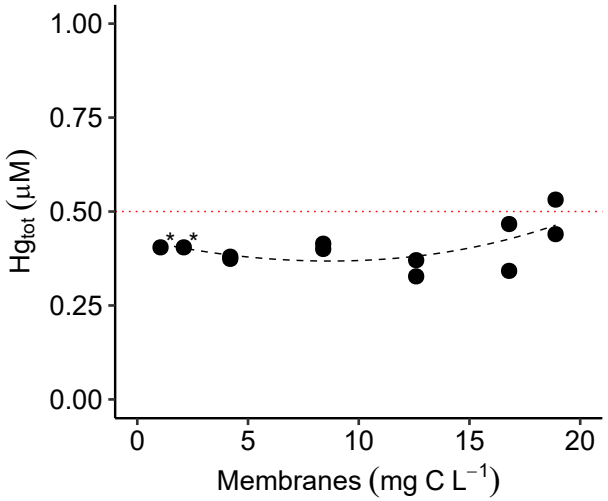

Figure S2: Hg_{tot} as a function of *Geobacter* membrane concentration in the competitive ligand exchange experiments. The black circles represent measured concentrations of Hg_{tot} and the red dotted line represents the theoretically added Hg concentration of 0.5 μM. Please note that Hg_{tot} in samples of 1 and 2 mg C L^{-1} (labeled by *) were not measured thus the average value 0.4 μM was used.

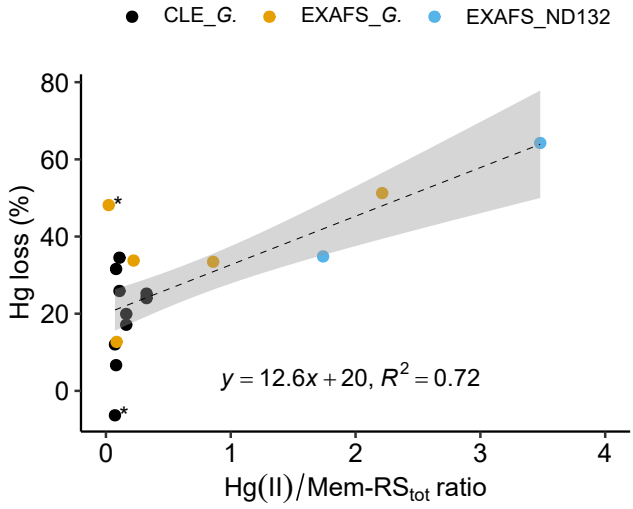

Figure S3: Loss of Hg(II) as a function of Hg(II)/Mem-RS_{tot} molar ratio in the Competitive Ligand Exchange experiments of membranes *Geobacter* (CLE_*G.*), Hg L_{III}-edge EXAFS experiments of membranes *Geobacter* (EXAFS_*G.*) and ND132 (EXAFS_ND132). * denotes two outliers, and the gray shaded area represents the 95% confidence interval of the fitted linear equation with the two outliers excluded.

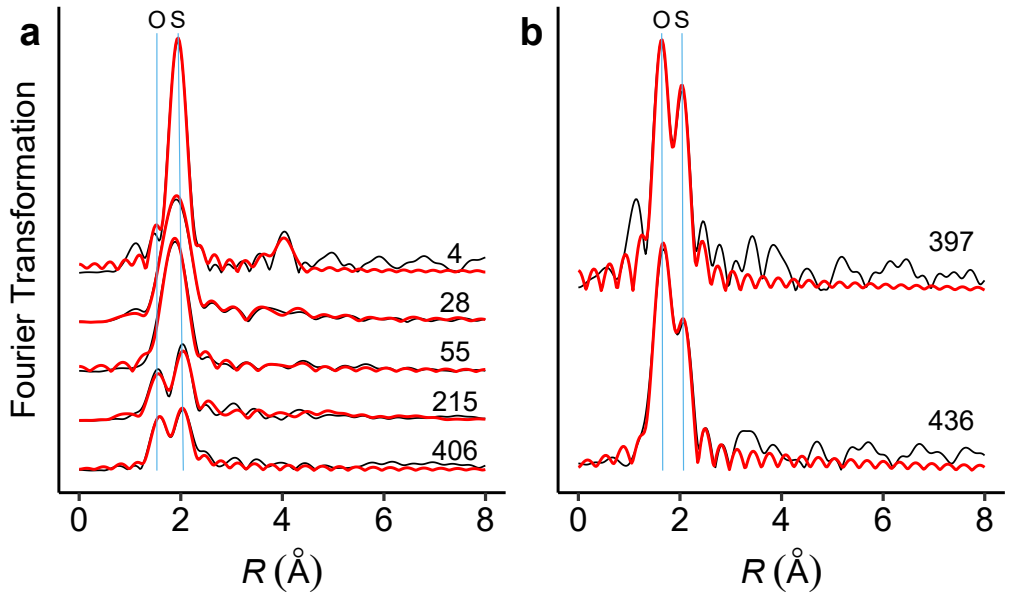

Figure S4: Fourier-transformed Hg L_{III}-edge EXAFS *R*-space spectra (black lines) and model fits (red lines) of isolated membrane samples of (a) *Geobacter* and (b) ND132. Numbers on the right side above each spectrum represent Hg_{tot} concentrations (μmol g^{-1} C) determined after samples had been subjected to EXAFS measurements. The blue vertical lines indicate Hg−O/N and Hg−S bond distances uncorrected for phase shift.

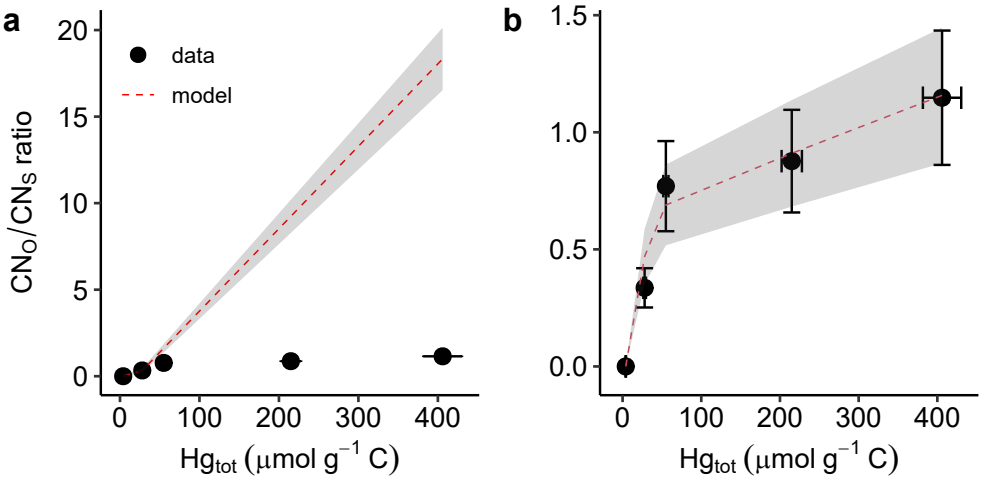

Figure S5: CN_S/CN_O ratio as a function of Hg_{tot} in *Geobacter* membranes samples determined by Hg L_{III}-edge EXAFS experiments and calculations using (a) a simple model NOM samples and (b) a more complex model (See text in SI). The error bars and gray area represents ± 25% uncertainty of measured and modeled CN_S/CN_O ratios, respectively.

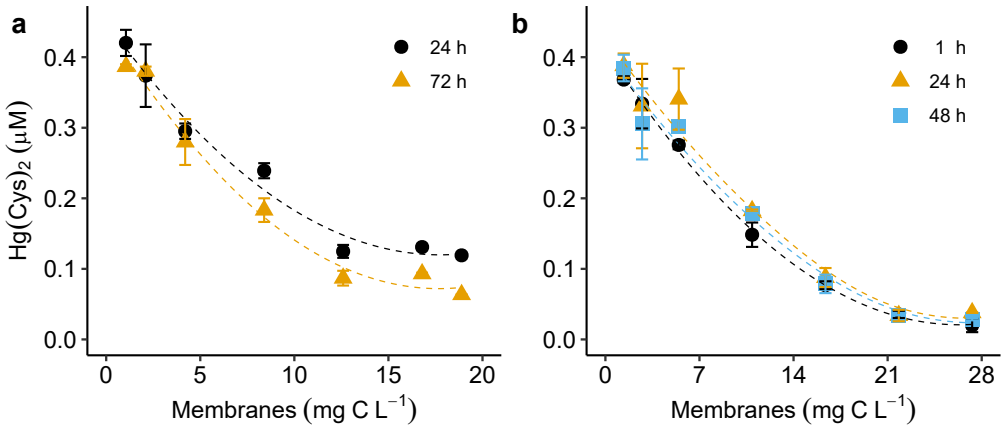

Figure S6: The concentration of $Hg(Cys)_2$ as a function of membrane concentration of (a) *Geobacter* and (b) ND132 at different reaction times (1, 24 and 72 h) after Cys addition in competitive ligand exchange experiments. Experiments were conducted at pH ~4.0 and I = 10 mM $NaClO_4$ by pre-equilibrating 0.5 μM $Hg(NO_3)_2$ with different concentration of bacterium membranes for 24 h before addition of 2.0 μM Cys. The difference in $Hg(Cys)_2$ concentration at different reaction times was not significant ($p > 0.05$, ANOVA, Tukey-HSD).

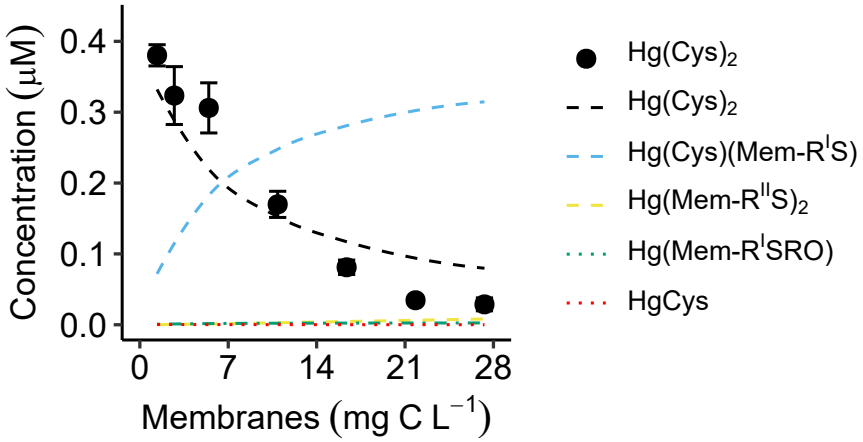

Figure S7: Experimentally determined $Hg(Cys)_2$ concentrations (± SD, $n = 6$) as a function of ND132 membrane concentrations in competitive ligand exchange experiments. Experiments were conducted at pH ~4.0 and I = 10 mM $NaClO_4$ by pre-equilibrating 0.5 μM $Hg(NO_3)_2$ with different concentrations of bacterium membrane (1–27 mg C L^{-1} corresponding to 0.5–9.6 μM of Mem-RS_{tot}) for 24 h followed by Cys addition to yield 2.0 μM. Dashed black line represents the modeled $Hg(Cys)_2$ concentration. The model was optimized by R software using the PHREEQC package obtaining a minimum merit-of-fit, $\sum(Model - Experiment)^2/\sum Experiment^2$, of 5%.

References

(S1) Caccavo, F.; Lonergan, D. J.; Lovley, D. R.; Davis, M.; Stolz, J. F.; McInerney, M. J. Geobacter Sulfurreducens Sp. Nov., a Hydrogen-and Acetate-Oxidizing Dissimilatory Metal-Reducing Microorganism. *Appl Env. Microbiol* **1994**, *60*, 3752–3759.

(S2) Schaefer, J. K.; Morel, F. M. High Methylation Rates of Mercury Bound to Cysteine by Geobacter Sulfurreducens. *Nat Geosci* **2009**, *2*, 123–126.

(S3) Schaefer, J. K.; Rocks, S. S.; Zheng, W.; Liang, L.; Gu, B.; Morel, F. M. M. Active Transport, Substrate Specificity, and Methylation of Hg(II) in Anaerobic Bacteria. *Proc. Natl. Acad. Sci. U.S.A.* **2011**, *108*, 8714–8719.

(S4) Gorby, Y. A.; Beveridge, T. J.; Blakemore, R. P. Characterization of the Bacterial Magnetosome Membrane. *J. Bacteriol.* **1988**, *170*, 834–841.

(S5) Sandrini, S. M.; Haigh, R.; Freestone, P. P. Fractionation by Ultracentrifugation of Gram Negative Cytoplasmic and Membrane Proteins. *Bio-Protoc.* **2014**, *4*, e1287.

(S6) Xia, K.; Weesner, F.; Bleam, W. F.; Bloom, P. R.; Skyllberg, U. L.; Helmke, P. A. XANES Studies of Oxidation States of Sulfur in Aquatic and Soil Humic Substances. *Soil Sci Soc Am J* **1998**, *62*, 1240–1246.

(S7) Ravel, B.; Newville, M. ATHENA, ARTEMIS, HEPHAESTUS: Data Analysis for X-Ray Absorption Spectroscopy Using IFEFFIT. *J Synchrotron Radiat* **2005**, *12*, 537–541.

(S8) Yekta, S. S.; Gustavsson, J.; Svensson, B. H.; Skyllberg, U. Sulfur K-Edge XANES and Acid Volatile Sulfide Analyses of Changes in Chemical Speciation of S and Fe during Sequential Extraction of Trace Metals in Anoxic Sludge from Biogas Reactors. *Talanta* **2012**, *89*, 470–477.

(S9) Song, Y.; Jiang, T.; Liem-Nguyen, V.; Sparrman, T.; Björn, E.; Skyllberg, U. Thermodynamics of Hg(II) Bonding to Thiol Groups in Suwannee River Natural Organic Matter Resolved by Competitive Ligand Exchange, Hg L_{III}-Edge EXAFS and ^{1}H NMR Spectroscopy. *Environ. Sci. Technol.* **2018**, *52*, 8292–8301.

(S10) Hayama, S.; Duller, G.; Sutter, J. P.; Amboage, M.; Boada, R.; Freeman, A.; Keenan, L.; Nutter, B.; Cahill, L.; Leicester, P.; Kemp, B.; Rubies, N.; Diaz-Moreno, S. The Scanning Four-Bounce Monochromator for Beamline I20 at the Diamond Light Source. *J. Synchrotron Radiat.* **2018**, *25*, 1556–1564.

(S11) Ressler, T. WinXAS: A Program for X-Ray Absorption Spectroscopy Data Analysis under MS-Windows. *J Synchrotron Radiat* **1998**, *5*, 118–122.

(S12) Rehr, J. J.; Booth, C. H.; Bridges, F.; Zabinsky, S. I. X-Ray-Absorption Fine Structure in Embedded Atoms. *Phys Rev B Condens Matter* **1994**, *49*, 12347–12350.

(S13) Zabinsky, S. I.; Rehr, J. J.; Ankudinov, A.; Albers, R. C.; Eller, M. J. Multiple-Scattering Calculations of x-Ray-Absorption Spectra. *Phys Rev B Condens Matter* **1995**, *52*, 2995–3009.

(S14) Skyllberg, U.; Bloom, P. R.; Qian, J.; Lin, C.-M.; Bleam, W. F. Complexation of Mercury(II) in Soil Organic Matter: EXAFS Evidence for Linear Two-Coordination with Reduced Sulfur Groups. *Environ. Sci. Technol.* **2006**, *40*, 4174–4180.

(S15) Serudo, R. L.; de Oliveira, L. C.; Rocha, J. C.; Paterlini, W. C.; Rosa, A. H.; da Silva, H. C.; Botero, W. G. Reduction Capability of Soil Humic Substances from the Rio Negro Basin, Brazil, towards Hg(II) Studied by a Multimethod Approach and Principal Component Analysis (PCA). *Geoderma* **2007**, *138*, 229–236.

(S16) Gu, B.; Bian, Y.; Miller, C. L.; Dong, W.; Jiang, X.; Liang, L. Mercury Reduction and Complexation by Natural Organic Matter in Anoxic Environments. *PNAS* **2011**, *108*, 1479–1483.

(S17) Zheng, W.; Liang, L.; Gu, B. Mercury Reduction and Oxidation by Reduced Natural Organic Matter in Anoxic Environments. *Environ. Sci. Technol.* **2012**, *46*, 292–299.

(S18) Jiang, T.; Skyllberg, U.; Wei, S.; Wang, D.; Lu, S.; Jiang, Z.; Flanagan, D. C. Modeling of the Structure-Specific Kinetics of Abiotic, Dark Reduction of Hg(II) Complexed by O/N and S Functional Groups in Humic Acids While Accounting for Time-Dependent Structural Rearrangement. *Geochim Cosmochim Acta* **2015**, *154*, 151–167.

(S19) Joe-Wong, C.; Shoenfelt, E.; Hauser, E. J.; Crompton, N.; Myneni, S. C. B. Estimation of Reactive Thiol Concentrations in Dissolved Organic Matter and Bacterial Cell Membranes in Aquatic Systems. *Environ. Sci. Technol.* **2012**, *46*, 9854–9861.

(S20) Yu, Q.; Szymanowski, J.; Myneni, S. C. B.; Fein, J. B. Characterization of Sulfhydryl Sites within Bacterial Cell Envelopes Using Selective Site-Blocking and Potentiometric Titrations. *Chem Geol* **2014**, *373*, 50–58.

(S21) Nell, R. M.; Fein, J. B. Influence of Sulfhydryl Sites on Metal Binding by Bacteria. *Geochim Cosmochim Acta* **2017**, *199*, 210–221.

(S22) Hu, H.; Lin, H.; Zheng, W.; Rao, B.; Feng, X.; Liang, L.; Elias, D. A.; Gu, B. Mercury Reduction and Cell-Surface Adsorption by Geobacter Sulfurreducens PCA. *Environ. Sci. Technol.* **2013**, *47*, 10922–10930.

(S23) Lin, H.; Morrell-Falvey, J. L.; Rao, B.; Liang, L.; Gu, B. Coupled Mercury-Cell Sorption, Reduction, and Oxidation on Methylmercury Production by Geobacter Sulfurreducens PCA. *Environ. Sci. Technol.* **2014**, *48*, 11969–11976.

(S24) Wang, Y.; Schaefer, J. K.; Mishra, B.; Yee, N. Intracellular Hg(0) Oxidation in Desulfovibrio Desulfuricans ND132. *Env. Sci Technol* **2016**, *50*, 11049–11056.

(S25) Liem-Nguyen, V.; Skyllberg, U.; Nam, K.; Björn, E. Thermodynamic Stability of Mercury(II) Complexes Formed with Environmentally Relevant Low-Molecular-Mass Thiols Studied

by Competing Ligand Exchange and Density Functional Theory. *Environ. Chem.* **2017**, *14*, 243–253.

(S26) Skyllberg, U. Competition among Thiols and Inorganic Sulfides and Polysulfides for Hg and MeHg in Wetland Soils and Sediments under Suboxic Conditions: Illumination of Controversies and Implications for MeHg Net Production. *J. Geophys. Res. Biogeosciences* **2008**, *113*, 1–14.

(S27) Mishra, B.; Shoenfelt, E.; Yu, Q.; Yee, N.; Fein, J. B.; Myneni, S. C. B. Stoichiometry of Mercury-Thiol Complexes on Bacterial Cell Envelopes. *Chem Geol* **2017**, *464*, 137–146.

(S28) Thomas, S. A.; Mishra, B.; Myneni, S. C. Cellular Mercury Coordination Environment, and Not Cell Surface Ligands, Influence Bacterial Methylmercury Production. *Environ. Sci. Technol.* **2020**, *54*, 3960–3968.

(S29) Rao, B.; Simpson, C.; Lin, H.; Liang, L.; Gu, B. Determination of Thiol Functional Groups on Bacteria and Natural Organic Matter in Environmental Systems. *Talanta* **2014**, *119*, 240–247.